

## Article

# Application of the AMT Method to Gold Deposits: A Case Study in the Qinling Metallogenic Belt of North China Craton

Fengchun Li <sup>1,2,3</sup> , Qingdong Zeng <sup>1,2,3,\*</sup>, Rixiang Zhu <sup>2,3,4</sup>, Shaoxiong Chu <sup>1,2</sup>, Wei Xie <sup>1,2,3</sup>, Bolin Zhang <sup>5</sup> and Xingxing Zhang <sup>5</sup>

- <sup>1</sup> Key Laboratory of Mineral Resources, Institute of Geology and Geophysics, Chinese Academy of Sciences, Beijing 100029, China; lifengchun20@mails.ucas.ac.cn (F.L.); chushaoxiong@mail.iggcas.ac.cn (S.C.); xiewei20@mails.ucas.ac.cn (W.X.)
- <sup>2</sup> Innovation Academy for Earth Science, Chinese Academy of Sciences, Beijing 100029, China; rxzhu@mail.iggcas.ac.cn
- <sup>3</sup> University of Chinese Academy of Sciences, Beijing 100049, China
- <sup>4</sup> State Key Laboratory of Lithospheric Evolution, Institute of Geology and Geophysics, Chinese Academy of Sciences, Beijing 100029, China
- <sup>5</sup> Lushi Zhongke Mining Co., Ltd., Sanmengxia 472200, China; zbl10086@gmail.com (B.Z.); zhangxingxing2021@gmail.com (X.Z.)
- \* Correspondence: zengqingdong@mail.iggcas.ac.cn; Tel.: +86-010-8299-8175

**Abstract:** The Lushi gold polymetallic ore-concentration area, located in the southern margin of North China Craton, is an important polymetallic ore district in the Qinling metallogenic belt. The Jianbeigou gold deposit is an important quartz vein type gold deposit in this district. In order to reveal the geological structure of the Jianbeigou gold deposit to guide deep prospecting, the EH4 conductivity image system was used in the Jianbeigou area. The sections obtained by the audio magnetotellurics method (AMT) indicate that the steeply dipping low resistivity zone in the area has a good corresponding relationship with the location of the known shallow ore bodies, and an extension in the deep. The low resistivity anomaly zone obtained by the inversion results are well correlated with the gold mineralization zone of the ore bodies, indicating good deep prospecting and exploration potential in this area. Based on geological and geophysical evidences, this paper inferred the possible occurrence location and depth range of the buried ore bodies. The AMT survey results reflect good exploration potential of the mining area and provide a geophysical basis for deep prospecting.

**Keywords:** EH4 conductivity image system; Jianbeigou gold deposit; deep prospecting; Qinling metallogenic belt



**Citation:** Li, F.; Zeng, Q.; Zhu, R.; Chu, S.; Xie, W.; Zhang, B.; Zhang, X. Application of the AMT Method to Gold Deposits: A Case Study in the Qinling Metallogenic Belt of North China Craton. *Minerals* **2021**, *11*, 1200. <https://doi.org/10.3390/min11111200>

Academic Editor: Stanisław Mazur

Received: 9 October 2021

Accepted: 26 October 2021

Published: 28 October 2021

**Publisher's Note:** MDPI stays neutral with regard to jurisdictional claims in published maps and institutional affiliations.



**Copyright:** © 2021 by the authors. Licensee MDPI, Basel, Switzerland. This article is an open access article distributed under the terms and conditions of the Creative Commons Attribution (CC BY) license (<https://creativecommons.org/licenses/by/4.0/>).

## 1. Introduction

The Qinling metallogenic belt, situated in the southern margin of the North China Craton (NCC), is one of the most important Au-Mo polymetallic ore belts in China, which is characterized by voluminous gold, molybdenum, and lead-zinc polymetallic deposits [1–3]. The Qinling metallogenic belt was formed under the complex crust–mantle interactions and the diverse metallogenic processes. A lot of super large-scale or large-scale gold and molybdenum ore-concentration areas such as Xiaoqinling and Xiong’ershan have been determined in this area [4–6] (Figure 1). The Qinling metallogenic belt, which is one of the largest large-scale deposit accumulation areas in the world, has attracted much attention due to its huge resource potential. Therefore, the Qinling metallogenic belt is regarded as a good metallogenic condition and exploration potential region [7]. However, the surface conditions of the Qinling metallogenic belt are complex and changeable, such as extensively developed surface folds and faults, mostly high-steep structures, harsh survey environments, and difficult field construction. Compared with other geophysical prospecting methods, the audio magnetotellurics method (AMT) has the unique advantages

of high observation efficiency, strong resolving power, portable instrument, and better resolution for low resistivity objects. Therefore, it is an effective method to study deep geological structures and explore hidden metal ore bodies.

In the past decades years, geophysical exploration technology has made significant progress in China [8–13]. The resolution and inversion interpretation capabilities of mid-deep mineral exploration have greatly improved especially, providing technical support for the fine detection of metal ore in second depth space (500–2000 m) [14]. The demand for mineral resources is growing, along with high country economy development. In order to achieve the sustainable development of the national economy and society, it is necessary to rapidly strengthen the prospecting, exploration, and resource development and utilization of the second depth space in the crust [15–18]. AMT has been applied to solid mineral exploration in the mid-deep because of its large detection depth, which is suitable for mineral resource exploration in the second space [19,20]. Also, it is widely used in the structural detection of ore field scale and the delineation of a metallogenic target area [21]. The AMT method played an important role in the exploration of deposits in China, like the discoveries of the Chaihulanzi gold concealed deposit, Inner Mongolia [22]; and the exploration of the interlayer slip breccia gold deposit in Pengjiakuang mine, Shandong Province [23]. Besides, this method has also been successfully applied for the prospecting of gold and lead–zinc deposits in the Tianshan–Xingmeng orogenic belt [24]. These applications have achieved a series of good results.

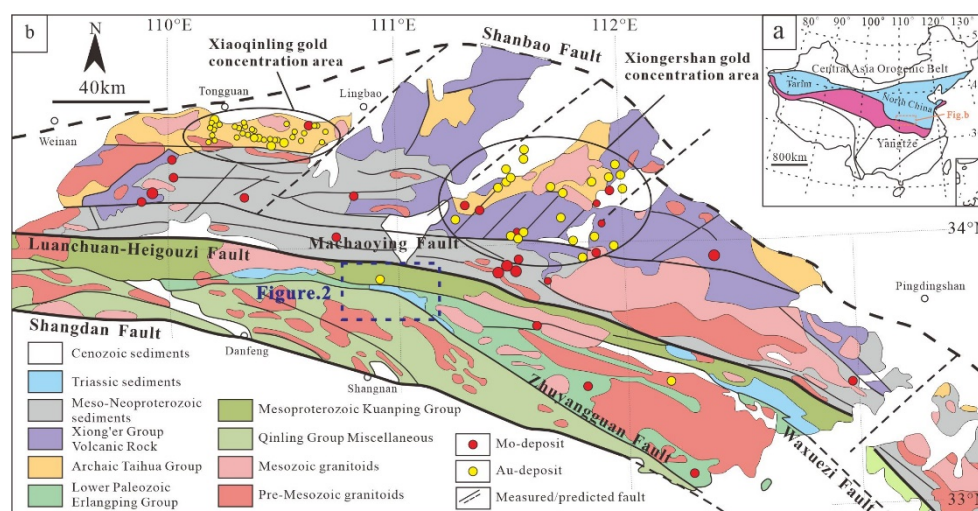


**Figure 1.** Geological map of the Eastern Qinling area on the southern margin of the NCC showing: (a) the position of the study area and distribution of Au deposits; (b) the position of the Eastern Qinling and other tectonic units, and distribution of Au deposits (Modified from [3,25,26]).

Due to its portable mode, no near-field effect, and high working efficiency, the EH4 conductivity image system is an ideal instrument for deep profiling of metal deposits in the Qinling metallogenic belt. This paper demonstrates application of the AMT method to the Jianbeigou gold deposit.

## 2. Geological Setting

The NCC is bounded by the Qinling-Dabie-Sulu Mesozoic orogenic belt in the south and the Xing-Meng Late Paleozoic orogenic belt in the north, and the eastern margin adjacent to the Pacific Plate [27]. From the early period to the Mesozoic, the NCC has undergone complex tectonic evolution. Tectonic regime transformation and crustal activation appeared in the NCC during Mesozoic, and the thinning of the lithosphere and the appearance of voluminous crust-derived granites were the main characteristics [28]. Previous studies have shown that the destruction of the craton and the Mesozoic magmatism in eastern North China are closely related to the subduction of the paleo-Pacific plate [29–31]. Since

the Early Jurassic, the paleo-Pacific plate has changed from a low-angle subduction to a high-angle subduction, accompanied by the retreat of the subduction zone, which induced strong destruction in the eastern part of the NCC. It caused large-scale tectonic-magmatic activities, and a large number of gold and other metal deposits were formed [32]. In the Early Devonian, the NCC collided with the North Qinling microcontinent [33,34]. The southern margin of the NCC and its adjacent Qinling Dabie metallogenic belt were in an extensional setting during Early Cretaceous in eastern China, forming a large-scale magmatic hydrothermal metallogenic system in the shallow [5]. It makes the Qinling metallogenic belt, where Lushi area is located, one of the important metallogenic areas in the tectonic-magmatic activity belt of the NCC.

The Lushi gold polymetallic ore-concentration area is situated in the southeastern part of the Qinling metallogenic belt. The geotectonic location spans two major structural units, the southern margin of the NCC and the Qinling orogenic belt (Figure 2). With superior ore-forming geological conditions, it is an important metal resource base in western Henan. In the Late Mesozoic, magmatic activity was extremely developed and it played an important role in the formation of contemporaneous endogenous metal minerals [35,36]. Quartz vein type gold deposits, structural altered rock-type gold deposits, porphyry-skarn type iron-copper polymetallic deposits, hydrothermal vein type copper-lead-zinc deposits, and rare metal pegmatites have developed in this ore-concentration area [37–39].

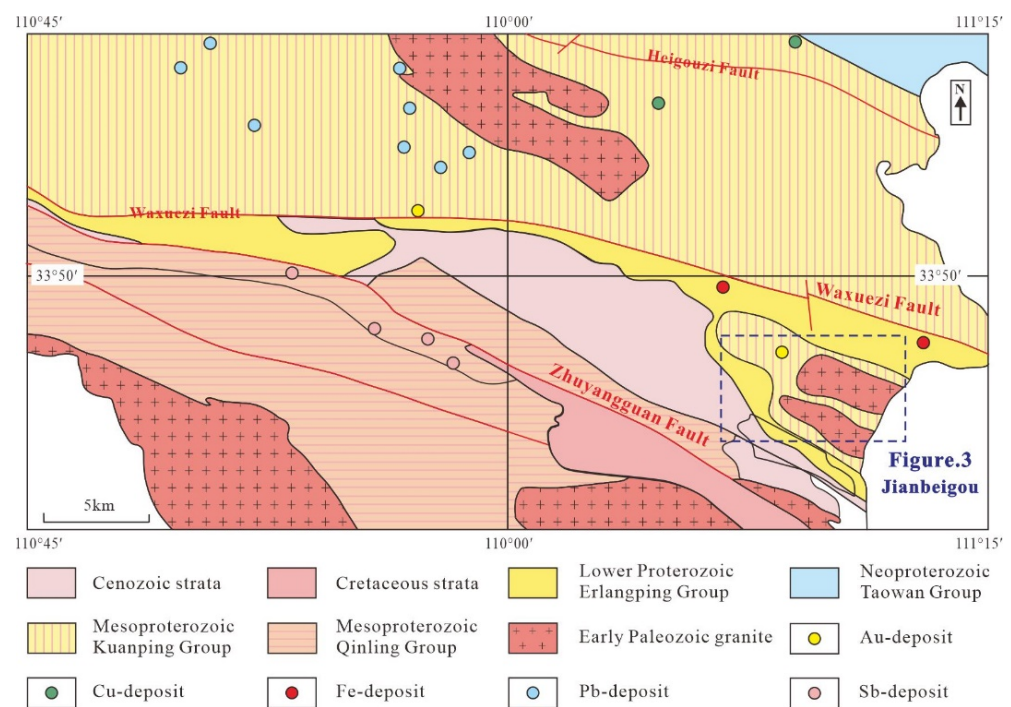


**Figure 2.** Geological map of Lushi gold polymetallic ore concentration area and distribution of metal deposits (Modified from [40]).

In the region, the strata of the NCC are situated in the northern section of the Luanchuan fault (Figure 1), which are characterized by a typical double-layer structure. The lower part is dominated by the Archean Taihua Group gneiss. Mesoproterozoic Xiong'er Group Volcanic rocks, Meso-Neoproterozoic sedimentary formations, and Meso-Cenozoic sedimentary formations make up the cover strata of the upper part. The strata of the North Qinling orogenic belt are seated in the southern section of the Luanchuan fault, which are composed of the Middle Proterozoic Qinling rock complex, Lower Paleozoic Erlangping Group sedimentary metamorphic rocks, Triassic marine strata, and Cenozoic sediments.

The overall geological structure of this area is NWW-trending, and each structural zone and structural unit is separated by large shear zones. The Waxuezi fault and the

Zhuyangguan fault are the major faults in this area. The Paleozoic granites are the mainly intrusive rocks in this area, and the Late Mesozoic intrusive rocks consisting of minor rock stocks are widely distributed in the north part of Heigouzi fault [41].

### 3. Jianbeigou Gold Deposit

The Jianbeigou gold deposit is situated between the Waxuezi fault and the Zhuyangguan fault (Figure 2). The deposit mainly occurs within the Lower Paleozoic Xiaozhai Formation (slate, sandstone) and consists of Au-bearing quartz veins and disseminated ore (Figure 3). The other strata mainly include the Lower Paleozoic Huoshenmiao Formation spilite keratophyre, Upper Triassic feldspathic quartz sandstone, carbonaceous slate, and the Quaternary sediments (Figure 3). The Au-bearing quartz veins are controlled by steeply dipping faults and the disseminated ores are dominated by the gently dipping interlayer fractured zone. The igneous rocks exposed in the area are Jianbeigou and Dongping plutons, both are gneissic granites.

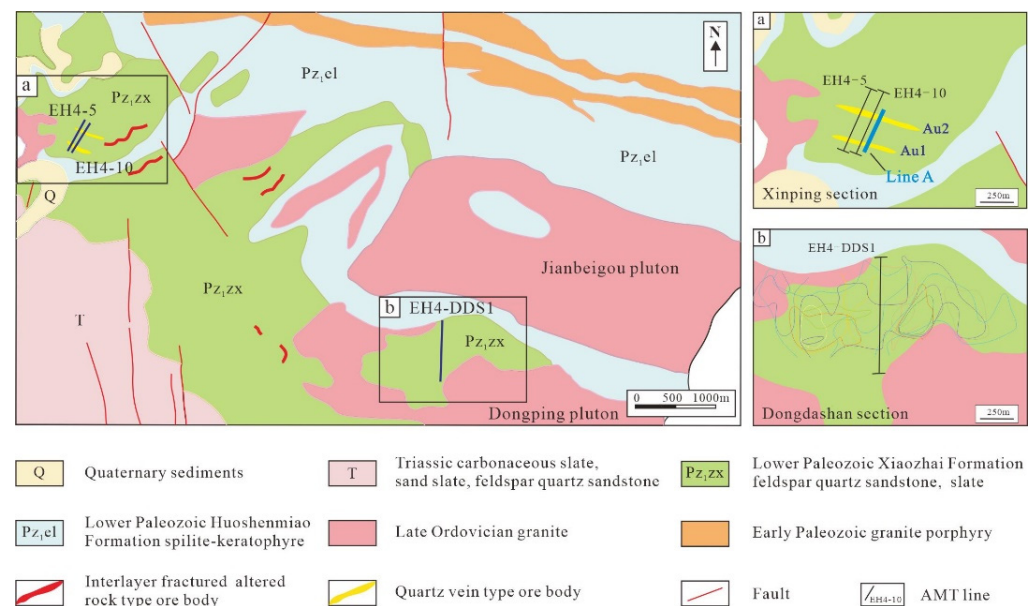


**Figure 3.** Geological map and the distribution of AMT survey lines in Jianbeigou gold deposit showing: (a) Line 10 and Line 5 in Xinping section; (b) Line DDS1 in Dongdashan section (Modified from [40]).

Two main groups of ore-bearing structures exist within this mining area. One group is a steeply dipping ore-bearing structure. The NWW-striking ore-controlling structures were observed to dip toward the north at angles of 75–85°. The main structure of this group occurred in the Early Paleozoic granite, and the early deformation of the structures was ductile shear deformation. The other group (interlayer fracture zone) is a gently dipping ore-bearing structure, with a dip angle of 0–20°.

The overall exploration level of the deposit is relatively low. The Xinping mine is only about 150 m deep (Figure 4). The contact between the Xiaozhai Formation and the Early Paleozoic granite is exposed at elevation of about 800 m above sea level (Figure 4). The presence of ore bodies (Au1 and Au2) on the study profile (Line A; Figure 3a) was indicated by ore bodies exposed in the Xinping mine. There are even less data for the Dongdashan mine section, except for geochemical anomalies of gold [40].

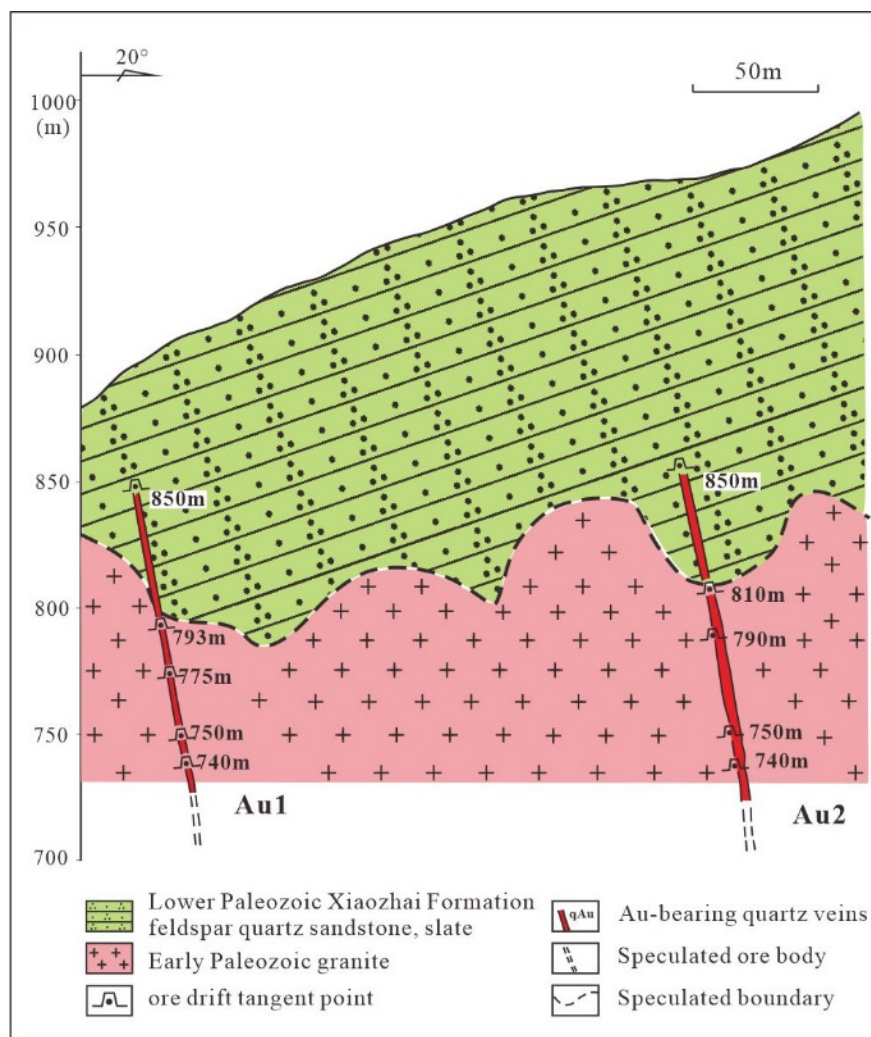


**Figure 4.** Xinping profile of tunnel control of the Au-bearing quartz veins in the Jianbeigou gold deposit (Modified from [40]).

The quartz veins are steep and the surrounding rocks are Early Paleozoic granites, as shown in Figure 5. Diabase dykes and quartz veins occur within the same ductile deformation ore-bearing structural belt. The banded structure formed by shearing in the ore-bearing veins can be clearly observed (Figure 5a,b). The contact surface between quartz vein and granite is straight, and ore boundaries are regular (Figure 5a,c). The gold-bearing quartz veins are white, greasy luster, with massive structure. The shapes of the disseminated ores are lenticular, sac-like, vein-like, lentil-like, beaded-like, and irregular (Figure 5d,e). The metallic minerals are mainly composed of pyrite, chalcopyrite, pyrrhotite, galena and sphalerite, with minor amounts of electrum detected (Figure 5b,d). The gangue minerals are mainly composed of sericite, quartz, calcite, and chlorite. The alteration types include silicification, chloritization, sericitization, and carbonatization.

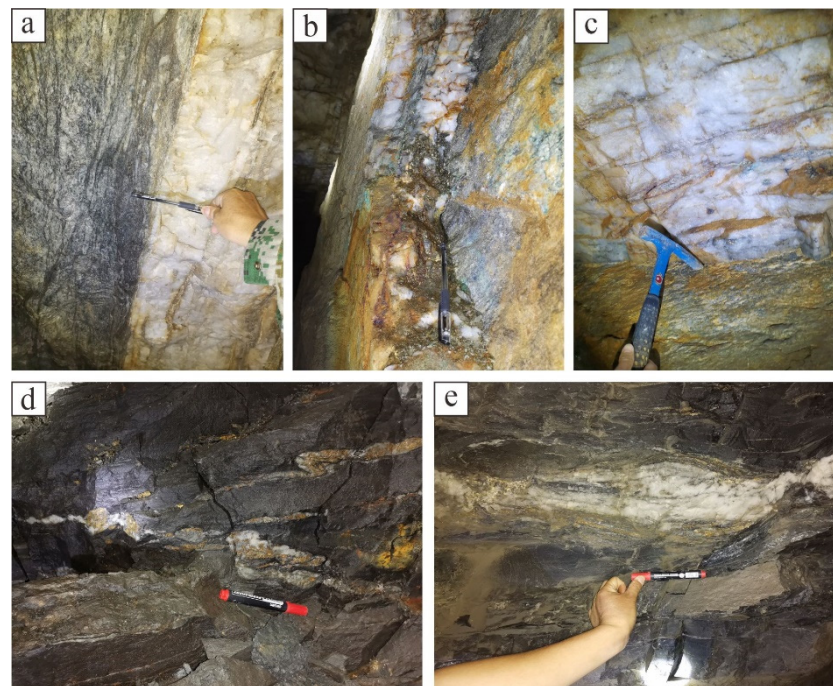


**Figure 5.** Photographs of ore bodies in the Jianbeigou deposit showing: (a) Au-bearing quartz veins controlled by ductile shear zone in granite; (b) quartz-polymetallic sulfide vein; (c) shear band structures developed in quartz veins; (d) sub-horizontal Au-bearing quartz vein; (e) lenticular vein body.

#### 4. Methodology

The electromagnetic method plays an important role in mineral exploration and has been widely used in searching for metal resources such as gold, copper, molybdenum, lead-zinc, bauxite, and uranium [42–44]. In this paper, detailed field geological surveys and AMT survey were carried out to investigate the Jianbeigou gold deposit in the Qinling metallogenic belt. The purpose of the AMT survey is to identify the resistivity characteristic of the gold ore bodies and the extension of ore-controlling structures (or ore bodies). In combination with the 850–700 m exploration adit prospecting project, two ore bodies Au1 and Au2 in the north-west trending ( $280^\circ$ ) were selected for AMT geophysical survey (Line 10 and Line 5). The target area with Au element geochemical anomaly was selected for the DDS1 line, and its mineralization fracture zone discussed.

##### 4.1. Experimental Method

Audio magnetotelluric sounding is an important geophysical method that uses natural electromagnetic fields as the field source to study the electrical structure of the earth's interior [45,46]. The earth is seen as the horizontal medium and the magnetotelluric field is vertically projected into the ground in the form of plane electromagnetic waves. Orthogonal electromagnetic field components are observed on the ground, and its frequency response reflects the vertical distribution of the electrical properties of the underground medium. Through a certain inversion method, the resistivity distribution at different depths can be obtained [47].

A mixed-source frequency domain electromagnetic sounding system, called the EH4 Conductivity Image Systems, was jointly produced by Geometrics and EMI in the 1990s [48]. It combines the advantages of both CSAMT and MT. The passive source electromagnetic method is the core, the natural background field source reflects the deep structure, and the artificial transmitted signal is the radiator to compensate for the shortcomings of some frequency bands of the natural signal. In areas with weak or no signal, it ensures that

a reliable signal can be observed in the entire frequency band to obtain high-resolution resistivity imaging [49].

The EH4 Conductive Image System realizes continuous acquisition of electromagnetic signals in the range of 0.1 Hz to 100 kHz. It can receive and analyze the electric and magnetic fields in both X and Y directions at the same time, and invert the X-Y conductivity tensor profile, which is particularly beneficial for judging the underground two-dimensional structure. It uses artificial electromagnetic fields (1–100 kHz) combined with natural electromagnetic fields (10 Hz–1 kHz) to measure earth resistivity. By first observing the orthogonal components of the electromagnetic field at the measuring point, the mutually orthogonal time-domain electric field components  $E_x$ ,  $E_y$ , and magnetic field components  $H_x$ ,  $H_y$  can be obtained, and the spatial attributes established. Then the time series data collected in the field can be edited to remove the time series fragments and obvious interference signals. For the measuring points curve, it can be smoothed or the frequency points with too large errors can be discarded, and the high-quality frequency point data retained. The variation of the magnetotelluric field component with time is converted into a frequency spectrum, and the magnetotelluric frequency domain response such as apparent resistivity and impedance phase can be calculated. Using the following expression:

$$\rho = (1/5f) |E_x/H_y|^2 \quad (1)$$

where,  $f$  is the frequency in Hz, and  $\rho$  is the resistivity in  $\Omega\text{m}$ .

The initial geoelectric model of the inversion process can use the apparent resistivity profile just obtained. The 2D analysis function (EMAP) was used to invert the measurement results and obtain the resistivity-depth profile.

#### 4.2. AMT Survey of the Jianbeigou Gold Deposit

Three EH4 profiles were carried out according to the geochemical anomaly characteristics and the geological characteristics of ore-controlling structures. The AMT survey lines are shown in the Figure 3. Measurement sites were set at 20 m intervals along with exploration lines. Among them, the EH4–5 line and the EH4–10 line were measured in the Xinping mine section, and the EH4–DDS1 line was measured in the Dongdashaan mine section for investigating the resistivity structures of the main mineralization belt (Figure 3). In order to eliminate the influence of terrain, the obtained sounding data were processed with terrain elevation correction. For AMT profile, the vertical axis is the altitude, the abscissa is the measurement point number, and the terrain line is obtained by interpolation using high-precision GPS data.

In this measurement, each electric field measurement point was soaked with clean water to reduce the contact resistivity of the detection point. Based on the analysis of the AMT data curve and the inversion resistivity model, the results show that the underground conductivity image of EH4 data inversion can display the deep extension of the ore-controlling shear structure and the variation characteristics of rock mass. It obviously reflects the differences in resistivity between the surrounding rock and the ore body. The resistivity of metal sulfide metallogenic belt is lower than host rocks such as intrusive rocks, granite, and metamorphic rocks. This geophysical information provides important and direct evidence for determining the location of concealed ore bodies in the study area.

### 5. Discussion

In this paper, Line 5 and Line 10 were measured on known shallow ore bodies. Their deep parts were extended and predicted in combination with geophysical methods. No ore bodies were previously investigated in the section of Line DDS1, but the metallogenic target area was circled by previous work using the primary halo geochemical method. The ore bearing fault zone were predicted and discussed to connect with this AMT survey. Considering its geological characteristics, prospecting engineering control characteristics, previous primary halo research results, and AMT measurement results, the three sections are discussed as follows.

### 5.1. AMT Survey Results and Imaging Data of EH4–10

The EH4–10 profile was measured in the middle of the Xinping mine section. The profile was 500 m in length, with 26 measurements set at 20 m intervals along with the north-eastern trending (at 15°). The inversion data of the EH4–10 line were plotted as a profile shown in Figure 6.

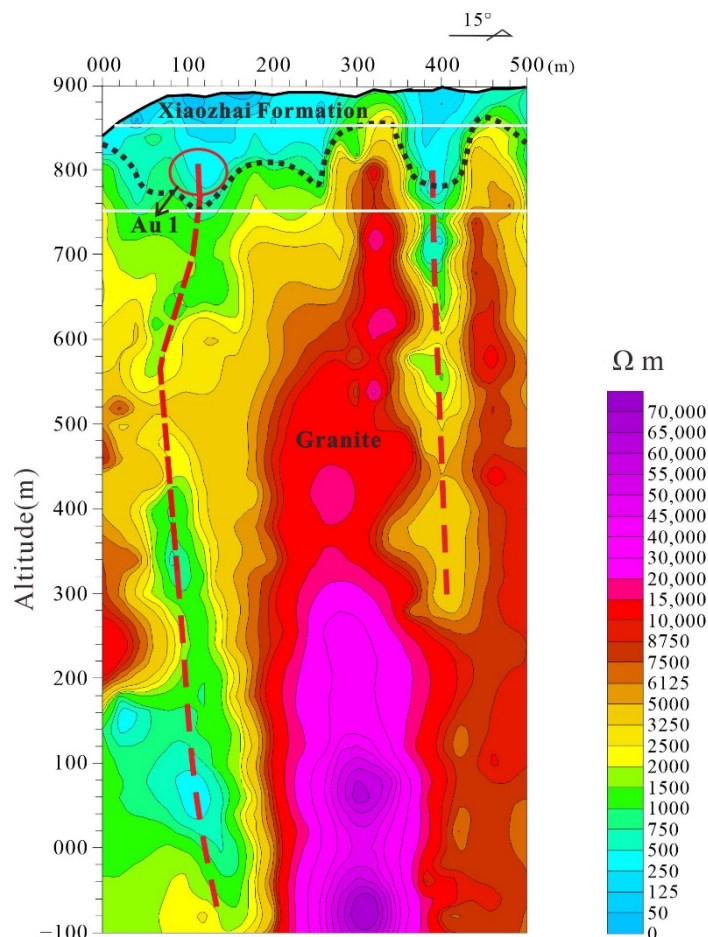


**Figure 6.** EH4 sounding image of Line 10 in the Xinping section of the Jianbeigou gold mine. The dashed line in the profile is the inferred geological boundary between the strata and the granite. The thick dashed red lines are the presumed mineralized zone. The thick, short solid red line is the known ore body location in the Xinping mine section. The white lines are the location of the exploration adit at 750 m and 850 m.

The inversion altitude of the AMT survey is 1000 m, and the minimum inversion altitude is −100 m. The AMT survey Line 10 (Figure 6) shows the following main features: (1) the low resistivity anomaly zone was mainly located in the shallow part of the section, and the high resistivity anomaly zone was known to occur within the deep part of the profile. (2) It is worth noting that there are two steeply dipping low resistivity anomaly belts in the high resistivity section, and the centers of the two low resistivity anomalies measured at 100 m and 360 m in the survey line, respectively.

It has been observed that the Xiaozhai Formation, which was mainly comprised of slate, schist, and bi-mica schist, was exposed in the 850 m exploration adit (white line). Occasionally, granite can be observed in the exploration adit. Thus, the low resistivity anomaly is presumed to be the geophysical response of the Lower Paleozoic Xiaozhai Formation, and the local resistivity increase at 280–340 m and 420–480 m is caused by shallow granite. This geological understanding of an investigated region is a good explanation for geophysical anomaly data.

The main ore body of the Xinping section consists of Early Paleozoic granite. At the same time, Early Paleozoic granite rock branches can be seen in the measured section of the surface, suggesting that granite still exists in the deep part of the section. Therefore, the mid-to-high resistance anomaly in the inverted section map is inferred and interpreted as the geophysical response of the Early Paleozoic granite.

Two large, steeply dipping, low resistivity zones in the inverted section are clearly highlighted from the surface down to the deep. The 100 m of the low resistivity zone was found to coincide with the location of a known ore body (Au1), which extended to a depth of about 1000 m. An Au1 ore body can be observed in the exploration adits of 740–850 m, as detailed at Figure 4. It has been observed that the shallow part of the low resistivity zone slopes steeply toward the south, and the deep part slopes steeply toward the north. In general, both the high resistivity zone and low resistivity zone dip toward the north. Thus, this low resistivity anomaly should be interpreted as the geophysical response of the Au1 quartz vein ore body, revealing that the Au1 ore body has a deep structural extension, showing good prospects for deep prospecting.

The 360 m of the low resistivity zone on the south side of the section was found to coincide with the location of a known Au2 ore body, which extended to a depth of about 650 m. Au2 ore body is controlled by the exploration adits of 740–850 m, as detailed at Figure 4. Consequently, it is assumed that the low resistivity anomaly zone is precisely related to the geophysical response of the Au2 quartz vein ore body. The Au2 ore body has a structural extension to a depth of more than 650 m, appearing a good prospect for deep prospecting. These findings also show no difference in this interpretation and the actual observations of the exploration adit. Meanwhile, it indicates that the low resistivity anomaly zone obtained by AMT inversion has a good correlation with the gold mineralization zone of the ore body.

## 5.2. AMT Survey Results and Imaging Data of EH4–5

In the present study, the EH4–5 profile was measured at the westernmost side of the Xinping mine section, which is 80 m away from the EH4–10 profile. Line 5 was 500 m in length, with 26 measurements at 20 m intervals along with the north-eastern trending (at 15°). The processing method of EH4 sounding data is the same as the EH4–10 profile. The obtained data of the EH4–5 line were plotted as a profile detailed in Figure 7.

The inversion altitude of the AMT survey is 1000 m, and the minimum inversion altitude is –100 m. It has been determined that the Lower Paleozoic Xiaozhai Formation was observed in the shallow part. It can be seen from the profile that the underground resistivity image along Line 5 is complex, especially at 260–460 m. Whereas, from the surface down to a depth of about 200 m, the resistivity presents a trend of gradually increasing. Based on appearance of the Lower Paleozoic Xiaozhai Formation, the low resistivity anomaly in the shallow part was caused by it. Following the completion of this geological survey, Early Paleozoic granite was found at an altitude of 830 m on the west side of the profile, indicating that the Xiaozhai Formation was under-embedded by the granite. The Xiaozhai Formation was limited in thickness and is less than 20 m. Thus, the high resistivity anomaly in the inverted profile at around 300 m is inferred and interpreted as the geophysical response of the Early Paleozoic granite.

The obtained resistivity section (Figure 7) showed that there were two resistivity anomalies located in the study area. The centers of the two low resistivity anomaly were measured at 100 m and 360 m, respectively. The 100 m point of the low resistivity zone was found to essentially correspond to the location of a known Au1 ore body in the mineralization belt. An Au1 ore body can be observed in the exploration adits of 740–850 m, as detailed at Figure 4. The shallow part of the low resistivity zone has a secondary low resistivity zone that slopes northward, and the deep part slopes steeply toward the north, extending to a depth of 1000 m. These findings show that the ore body has a structural extension in the deep. It was believed that this low resistivity anomaly represented the

possible location of a buried ore body. Also, a similarly resistive anomaly was found to exist at the 360 m mark. This is very important from the viewpoint of exploration prospectives.

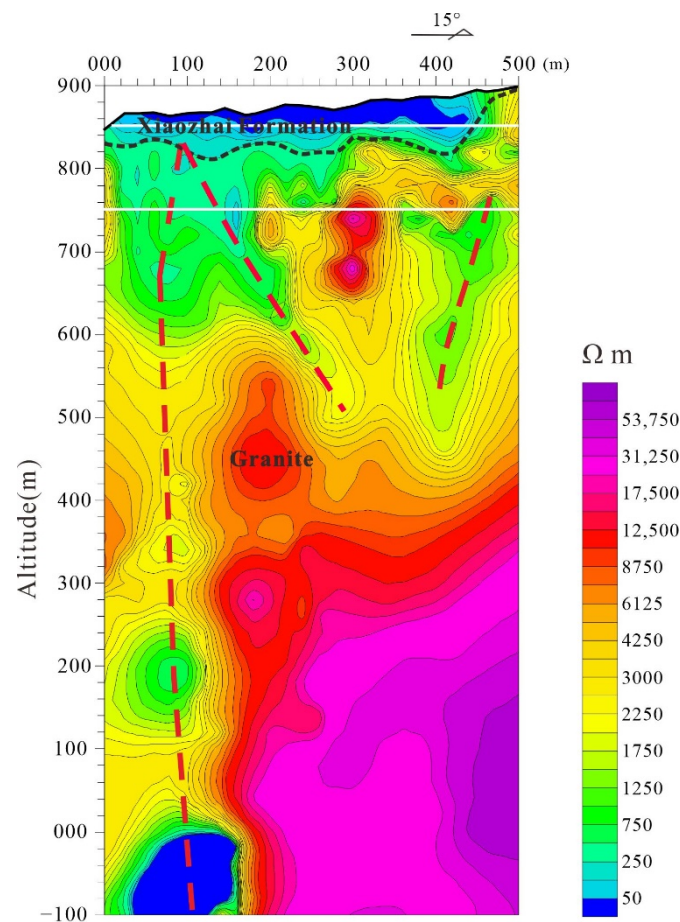


**Figure 7.** EH4 sounding image of Line 5 in the Xinping section of the Jianbeigou gold mine. The dashed line in the profile is the inferred geological boundary between the strata and the granite. The thick dashed red lines are the presumed mineralized zone. The white lines are the location of the exploration adit at 750 m and 850 m.

The resistivity model for the EH4–5 line was found to be similar to that of the EH4–10 line. However, the inverted profile has a good corresponding relationship with the actual position of the ore body. The 360 m of the low resistivity zone on the south side of the section was found to coincide with the location of a known Au2 ore body, which extended to a depth of about 500 m. The Au2 ore body is controlled by the exploration adits of 740–850 m, as detailed at Figure 4. Therefore, this low resistivity anomaly can be interpreted as being caused by the Au2 quartz vein ore body. Furthermore, the EH4 sounding image could strongly reveal that the gold-bearing mineralization belt was steeply dipping.

### 5.3. AMT Survey Results and Imaging Data of EH4–DDS1

In the current study, one EH4–DDS1 profile was measured in the Dongdashan mine section, which was 860 m in length. A total of 44 measurements sites were set at 20 m intervals along with the northern trending. The processing method of EH4 sounding data is the same as the EH4–10 profile. The obtained data of the EH4–DDS1 line were plotted as a profile detailed in Figure 8.

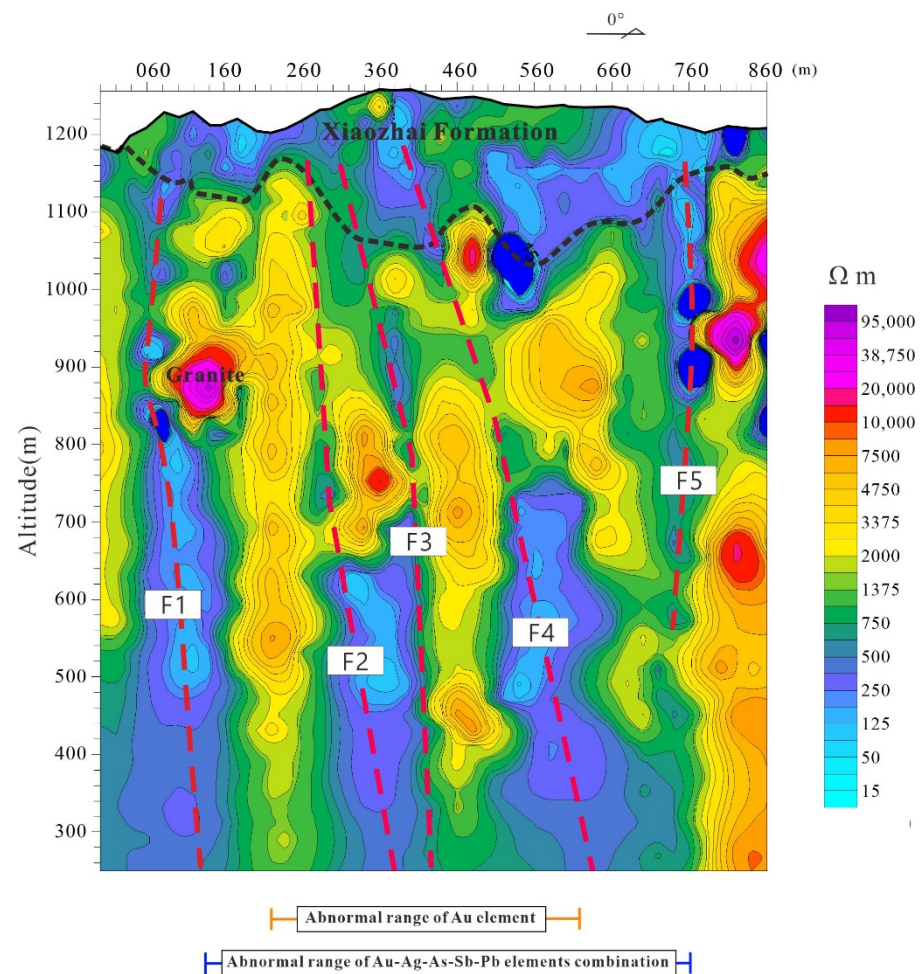


**Figure 8.** EH4 sounding image of Line DDS1 exploration line in the Dongdashan section of the Jianbeigou gold mine. The dashed line in the profile is the inferred geological boundary between the strata and the granite. The thick dashed red lines are ore-bearing abnormal structural belts.

The inversion altitude of the AMT profile is 1000 m, and the minimum inversion altitude is 260 m. The dotted line in the inversion profile is the inferred geological boundary between the strata and the granite. It was observed that Xiaozhai Formation, which was mainly composed of chlorite slate and mica schist, exists in the shallow part of this mining section. Also, granite was found on the south side of the section. From the surface down to a depth of about 100 m, the overall performance is low resistance; only minor amounts of resistivity increase at around 860 m. Therefore, the resistivity anomaly in the shallow part of the inverted profile is influenced by the Xiaozhai Formation and a small amount of exposed granite.

However, a medium-high resistivity anomaly background was also observed on the middle-deep part of the profile. Five low resistivity anomaly zones which dip steeply toward the north in the background were identified and numbered from south to north as F1–F5. The centers of low resistance anomalies are located at 60 m, 260 m, 280 m, 370 m, and 760 m, respectively. Based on the obtained results, it was inferred in this paper that the high resistivity zone of the mid-deep part caused by the Early Paleozoic granite, and the low resistivity anomaly is identified as the geophysical response of the low resistivity fault zone in the granite.

According to previous geochemical surveys [40], typical pathfinder element association (Ag-As-Sb-Pb) for gold ores [50] was indicated in the field, besides Au geochemical anomalies. The Au anomaly extends about 210–580 m across the survey Line DDS1 (N-S trending), including the F2–F4 fault zones. The width of the anomaly indicated by other

elements is wider, roughly 80–760 m in survey Line DDS1, and includes F1 and F5 fault zones. The presence and overlapping of the above-mentioned geochemical anomalies with fault zones indicated by the AMT method provide promise for the existence of Au-bearing ore zones. These, however, should be verified by drilling.

## 6. Conclusions

The following conclusions were reached in this paper:

- (1) In the exploration work of this research, the EH4 conductivity image system successfully identified the differences in resistivity between the host rock and the ore bodies. It is seen that the low resistivity anomaly zone in the AMT coincides with the known ore body in shallow exploration adit. The AMT results show a good extension of the known ore-controlling structures, which can reach a depth of 1000 m in the Xinping mine section and the possible existence of ore-bearing structures in the Dongdaishan mine section, which provides support for deep prospecting in this area.
- (2) The survey results indicated that the AMT method is effective and feasible in detecting the distribution of deep rock masses and strata in the Jianbeigou gold deposit in the Qinling metallogenic belt, China. The EH4 conductivity image system is an effective geophysical tool for detecting concealed metal deposits. It can provide basic geological information for deep resource exploration. This method can be used as an available exploration technology for deep prospecting in similar areas.

**Author Contributions:** Conceptualization, F.L. and Q.Z.; formal analysis, F.L.; investigation, F.L., Q.Z., B.Z. and X.Z.; resources, Q.Z. and R.Z.; writing—original draft preparation, F.L. and S.C.; writing—review and editing, Q.Z. and W.X.; visualization, F.L.; supervision, Q.Z.; funding acquisition, Q.Z. and R.Z. All authors have read and agreed to the published version of the manuscript.

**Funding:** This research was funded by the State Key Laboratory of Lithospheric Evolution, IGGCAS (SKL-Z201905).

**Acknowledgments:** We thank the leaders and technicians of Lushi Zhongke Mining Co., Ltd. and Jianbeigou Gold Mine for their great help and support during our field investigation in Lushi County. We are also grateful to anonymous reviewers for constructive suggestions.

**Conflicts of Interest:** The authors declare no conflict of interest.

## References

1. Mao, J.W.; Pirajno, F.; Xiang, J.F.; Gao, J.J.; Ye, H.S.; Li, Y.F.; Guo, B.J. Mesozoic molybdenum deposits in the east Qinling–Dabie orogenic belt: Characteristics and tectonic settings. *Ore Geol. Rev.* **2011**, *43*, 264–293. [[CrossRef](#)]
2. Li, J.W.; Bi, S.J.; Selby, D.; Chen, L.; Vasconcelos, P.; Thiede, D.; Zhou, M.F.; Zhao, X.F.; Li, Z.K.; Qiu, H.N. Giant Mesozoic gold provinces related to the destruction of the North China craton. *Earth Planet. Sci. Lett.* **2012**, *349–350*, 26–37. [[CrossRef](#)]
3. Li, N.; Chen, Y.J.; Pirajno, F.; Gong, H.J.; Mao, S.D.; Ni, Z.Y. LA-ICP-MS zircon U–Pb dating, trace element and Hf isotope geochemistry of the Heyu granite batholith, eastern Qinling, central China: Implications for Mesozoic tectono-magmatic evolution. *Lithos* **2012**, *142–143*, 34–47. [[CrossRef](#)]
4. Wang, R.T.; Qin, X.S.; Yuan, H.C.; Ding, K.; Wang, L.; Mao, J.W. Regional geochemistry, metallogenetic model and ore prospects of the western Xiaqingling Au–Mo polymetallic ore—Concentrated are, China. *Geol. Bull. China* **2021**, *40*, 531–544.
5. Zhao, X.F.; Li, Z.K.; Zhao, S.R.; Bi, S.J.; Li, J.W. Early Cretaceous Regional-Scale Magmatic-Hydrothermal Metallogenetic System at the Southern Margin of the North China Craton. *Earth Sci.* **2019**, *44*, 52–68.
6. Tang, K.F.; Li, J.W.; Selby, D.; Zhou, M.F.; Bi, S.J.; Deng, X.D. Geology, mineralization, and geochronology of the Qianhe gold deposit, Xiong’ershan area, southern North China Craton. *Miner. Depos.* **2013**, *48*, 729–747. [[CrossRef](#)]
7. Gao, S.; Zeng, Q.D.; Chu, S.X.; Zhou, T.C.; Fan, H.; Cheng, Z.D.; Ma, L.S. Fluid inclusions and stable isotopes study of Shuanghe Au deposit in western Henan. *Acta Petrol. Sin.* **2018**, *34*, 3539–3552.
8. Di, Q.; Xue, G.; Yin, C.; Li, X. New methods of controlled-source electromagnetic detection in China. *Sci. Chin. Earth Sci.* **2020**, *50*, 1219–1227. [[CrossRef](#)]
9. Di, Q.; Xue, G.; Lei, D.; Zeng, Q.; Fu, C.; An, Z. Summary of technology for a comprehensive geophysical exploration of gold mine in North China Craton. *Sci. Chin. Earth Sci.* **2021**, *64*, 1524–1536. [[CrossRef](#)]
10. Xue, G.Q.; Yan, S.; Chen, W.Y. A fast topographic correction method for electromagnetic data. *Chin. J. Geophys.* **2016**, *59*, 4408–4413.
11. Xue, G.; Zhang, L.; Hou, D.; Liu, H.; Ding, Y.; Wang, C.; Luo, X.; Xiao, W. Integrated geological and geophysical investigations for the discovery of deeply buried gold–polymetallic deposits in China. *Geol. J.* **2020**, *55*, 1771–1780. [[CrossRef](#)]

12. Xue, G.; Li, H.; He, Y.; Xue, J.; Wu, X. Development of the Inversion Method for Transient Electromagnetic Data. *IEEE Access* **2020**, *8*, 146172–146181. [[CrossRef](#)]
13. Wu, X.; Xue, G.; He, Y. The Progress of the Helicopter-Borne Transient Electromagnetic Method and Technology in China. *IEEE Access* **2020**, *8*, 32757–32766. [[CrossRef](#)]
14. Lu, Q.T.; Zhang, X.P.; Tang, J.T.; Jin, S.; Liang, L.Z.; Niu, J.J.; Wang, X.B.; Lin, P.R.; Yao, C.L.; Gao, W.L.; et al. Review on advancement in technology and equipment of geophysical exploration for metallic deposits in China. *Chin. J. Geophys.* **2019**, *62*, 3629–3664.
15. Teng, J.W.; Yang, L.Q.; Yao, J.Q.; Liu, H.C.; Liu, C.; Han, L.G.; Zhang, X.M. Deep discover ore, exploration and exploitation for metal mineral resources and its deep dynamical process of formation. *Chin. J. Geophys.* **2007**, *22*, 317–334.
16. Teng, J.W.; Yao, J.J.; Jiang, C.Z.; Yan, Y.F.; Yang, H.; Zhang, Y.Q.; Ruan, X.M. Magmatic rock mass and information for large and superlarge mineral deposits and its ore-prospecting effect in deep crust. *Acta Petrol. Sin.* **2009**, *25*, 1009–1038.
17. Yan, J.Y.; Teng, J.W.; Lu, Q.T. Geophysical exploration and application of deep metallic ore resources. *Prog. Geophys.* **2008**, *23*, 871–891.
18. Ye, Y.X.; Deng, J.Z.; Li, M.; Yang, H.Y. Application status and vistas of electromagnetic methods to deep ore prospecting. *Prog. Geophys.* **2011**, *26*, 327–334.
19. Zhai, Y.S.; Deng, J.; Wang, J.P.; Peng, R.M.; Liu, J.J.; Yang, L.Q. Researches on Deep Ore Prospecting. *Mineral. Depos.* **2004**, *23*, 142–149.
20. Feng, B.; Li, J.G.; Zhao, B.; Wang, Y.; Wang, J.L.; Zhang, J.F. The Application of Audio Magnetotelluric Method (AMT) in Nanling Yudu-Gan County Ore-Concentrated Area Yinkeng Demonstration Plot to Survey Deep Mineral Resources. *Acta Petrol. Sin.* **2014**, *88*, 669–675.
21. Tang, J.T.; Zhang, L.C.; Wang, X.Y.; Ren, Z.Y.; Zhou, C.; Zhao, W.G.; Wu, M.A. Subsurface electrical structure of the Fanshan-Jiangjunmiao area in the Lujiang-Zongyang Ore District derived from 3-D inversion of audio-magnetotelluric data. *Chin. J. Geophys.* **2018**, *61*, 1576–1587.
22. Liu, H.; Liu, J.; Yu, C.; Ye, J.; Zeng, Q. Integrated geological and geophysical exploration for concealed ores beneath cover in the Chaihulanzi goldfield, northern China. *Geophys. Prospect.* **2006**, *54*, 605–621. [[CrossRef](#)]
23. Qingdong, Z.; Yuanchao, S.; Tiebing, L.; Guangming, L.; Qirui, Z.; Kunfa, S.; Hongchen, L.; Xiuying, S.; Jinzhong, Y. Geophysical exploration for interlayer slip breccia gold deposits: Example from Pengjiakuang gold deposit, Shandong Province, China. *Geophys. Prospect.* **2004**, *52*, 97–108. [[CrossRef](#)]
24. Zeng, Q.; Di, Q.; Liu, T.; Li, G.; Yu, C.; Shen, P.; Liu, H.; Ye, J. Explorations of gold and lead-zinc deposits using a magnetotelluric method: Case studies in the Tianshan-Xingmeng Orogenic Belt of Northern China. *Ore Geol. Rev.* **2020**, *117*, 103283. [[CrossRef](#)]
25. Mao, J.W.; Xie, G.Q.; Pirajno, F.; Ye, H.S.; Wang, Y.B.; Li, Y.F.; Xiang, J.F.; Zhao, H.J. Late Jurassic–Early Cretaceous granitoid magmatism in Eastern Qinling, central-eastern China: SHRIMP zircon U–Pb ages and tectonic implications. *Aust. J. Earth Sci.* **2010**, *57*, 51–78. [[CrossRef](#)]
26. Gao, S. *Research on Mineralization of the Shuanghe Gold Deposit from the Western Henan, Southern Margin of the North China Craton*; University of Chinese Academy of Sciences: Beijing, China, 2018.
27. Hou, Z.Q.; Zheng, Y.C.; Geng, Y.S. Metallic refertilization of lithosphere along cratonic edges and its control on Au, Mo and REE ore systems. *Mineral. Depos.* **2015**, *34*, 641–674.
28. Zhai, M.G. Tectonic evolution of the North China Craton. *J. Geomech.* **2019**, *25*, 722–745.
29. Zhu, R.X.; Fan, H.R.; Li, J.W.; Meng, Q.R.; Li, S.R.; Zeng, Q.D. Decratonic gold deposits. *Sci. Chin. Earth Sci.* **2015**, *58*, 1523–1537. [[CrossRef](#)]
30. Tang, Y.J.; Ying, J.F.; Zhao, Y.P.; Xu, X.R. Nature and secular evolution of the lithospheric mantle beneath the North China Craton. *Sci. Chin. Earth Sci.* **2021**, *51*, 1489–1503.
31. Zhu, R.X.; Sun, W.D. The big mantle wedge and decratonic gold deposits. *Sci. Chin. Earth Sci.* **2021**, *51*, 1444–1456.
32. Yang, J.H.; Xu, L.; Sun, J.F.; Zeng, Q.D.; Zhao, Y.N.; Wang, H.; Zhu, Y.S. Geodynamics of decratonization and related magmatism and mineralization in the North China Craton. *Sci. Chin. Earth Sci.* **2021**, *51*, 1401–1419.
33. Zhang, C.L.; Liu, L.; Wang, T.; Wang, X.X.; Li, L.; Gong, Q.F.; Li, X.F. Granitic magmatism related to early Paleozoic continental collision in North Qinling. *Chin. Sci. Bull.* **2013**, *58*, 4405–4410. [[CrossRef](#)]
34. Dong, Y.P.; Santosh, M. Tectonic architecture and multiple orogeny of the Qinling Orogenic Belt, Central China. *Gondwana Res.* **2016**, *29*, 1–40. [[CrossRef](#)]
35. Gao, X.Y.; Zhao, T.P. Late Mesozoic magmatism and tectonic evolution in the Southern margin of the North China craton. *Sci. Chin. Earth Sci.* **2017**, *47*, 1309–1328. [[CrossRef](#)]
36. Zhao, T.P.; Meng, L.; Gao, X.Y.; Jin, C.; Wu, Q.; Bao, Z.W. Late Mesozoic felsic magmatism and Mo–Au–Pb–Zn mineralization in the southern margin of the North China Craton: A review. *J. Asian Earth Sci.* **2018**, *161*, 103–121. [[CrossRef](#)]
37. Zhang, Z.M.; Zeng, Q.D.; Gao, S.; Chu, S.X.; Li, D.T.; Cheng, Z.D.; Ma, L.S.; Guo, Y.P. The Rb–Sr isotopic dating of sulfides and geological significance of the Lushi polymetallic ore-concentrated area in southern margin of the North China Craton. *Acta Petrol. Sin.* **2019**, *35*, 2013–2025.
38. Zhou, Q.F.; Qin, K.Z.; Tang, D.W.; Wang, C.L.; Ma, L.S. Mineralogical characteristics and significance of beryl from the rare-element pegmatites in the Lushi County, East Qinling, China. *Acta Petrol. Sin.* **2019**, *35*, 1999–2012.

39. Zhou, D.; Bao, Z.W.; Yao, J.M.; Zeng, L.J.; Zhao, T.P. Chemistry of Pyrites from Babaoshan Iron and Copper Polymetallic Ore Deposit in Western Henan Province. *Geotecton. Metallog.* **2015**, *39*, 128–138.
40. Exploration, L.C.I.O.G. *Production and Exploration Report of Jianbeigou Gold Mine, Lushi County Institute of Geological Exploration, Henan Province 2011*; Lushi County Institute of Geological Exploration: Lushi, China, 2011. (In Chinese)
41. Hu, H.; Li, J.W.; Deng, X.D. LA-ICP-MS zircon U-Pb dating of granitoid intrusions related to iron-copper polymetallic deposits in Luonan-Lushi area of southern North China Craton and its geological implications. *Mineral. Depos.* **2011**, *30*, 979–1001.
42. Liu, J.X.; Sun, H.L.; Chen, B.; Guo, R.W. Review of the gravity and magnetic methods in the exploration of metal deposits. *Prog. Geophys.* **2016**, *31*, 713–722.
43. Guo, Z.W.; Xue, G.Q.; Liu, J.X.; Wu, X. Electromagnetic methods for mineral exploration in China: A review. *Ore Geol. Rev.* **2020**, *118*, 103357. [[CrossRef](#)]
44. Di, Q.Y.; Zhu, R.X.; Xue, G.Q.; Yin, C.C.; Li, X. New development of the Electromagnetic (EM) methods for deep exploration. *Chinese J. Geophys.* **2019**, *62*, 2128–2138.
45. Jones, A.G.; Garcia, X. Okak Bay AMT data-set case study: Lessons in dimensionality and scale. *Geophysics* **2003**, *68*, 70–91. [[CrossRef](#)]
46. Singh, R.K.; Maurya, V.P.; Singh, S. Imaging Regional Geology and Au—Sulphide mineralization over Dhanjori greenstone belt: Implications from 3-D Inversion of Audio Magnetotelluric data and Petrophysical Characterization. *Ore Geol. Rev.* **2019**, *106*, 369–386. [[CrossRef](#)]
47. Zhang, X.D.; Meng, X.H.; Chen, Z.X.; Wang, J.; Xiu, C.X. Comprehensive study of the geological and geophysical characteristics of the metallogenic belt in Southwest Fujian-A case study in the Yongding-Dapai polymetallic ore deposit. *Chin. J. Geophys.* **2018**, *61*, 1588–1595.
48. Chen, W.J.; Liu, H.T. Integrated geophysical exploration for concealed ore beneath cover in the Zhaojiangweizi area, Inner Mongolia, northern China. *Prog. Geophys.* **2009**, *24*, 293–302.
49. Liu, J.X.; Dong, X.Z.; Guo, R.W.; Li, A.Y.; Yang, S. *Magnetotelluric Sounding Exploration—Data Processing, Inversion and Interpretation*; Science Press: Beijing, China, 2012.
50. Goldberg, I.S.; Abramson, G.Y.; Los, V.L. Depletion and enrichment of primary haloes: Their importance in the genesis of and exploration for mineral deposits. *Geochem. Explor. Environ. Anal.* **2003**, *3*, 281–293. [[CrossRef](#)]